A 3D Ultrasound Robotic Prostate Brachytherapy System with Prostate Motion Tracking

Nikolai Hungr, Michael Baumann, Jean-Alexandre Long, Jocelyne Troccaz

A 3D Ultrasound Robotic Prostate Brachytherapy System with Prostate Motion Tracking

Nikolai Hungr, MASc, Michael Baumann, PhD, Jean-Alexandre Long, MD, MSc, Jocelyne Troccaz, PhD *Member, IEEE*

***Abstract*— This paper describes a new three-dimensional (3D) ultrasound robotic prostate brachytherapy system. It uses a stationary 3D ultrasound probe rigidly fixed to a robotic needle insertion mechanism. The novelty of the system is its ability to track prostate motion intra-operatively to allow the dose planning and needle trajectories or depths to be adapted to take into account these motions. Prostate tracking is done using a fast 3D ultrasound registration algorithm previously validated for biopsy guidance. The 7 degree of freedom robot and ultrasound probe are calibrated together with an accuracy of 0.9mm, allowing the needles to be precisely inserted to the seed targets chosen in the reference ultrasound image. Experiments were conducted on mobile and deformable synthetic prostate phantoms, using a prototype laboratory system. Results showed that, with prostate motions of up to 7mm, the system was able to reach the chosen targets with less than 2mm accuracy in the needle insertion direction. This measured accuracy included extrinsic measurement errors of up to about 1.1mm. A preliminary cadaver feasibility study was also described, in preparation for more realistic experimentation of the system.**

***Index Terms*— Robotic brachytherapy, Prostate motion tracking, Prostate registration, 3D ultrasound guidance, Medical robots and systems, Mechanism design.**

I. Introduction

THE prostate gland is one of the most commonly cancer-affected male organs in western developed countries. In 2012, 241 740 new cases of prostate cancer and 28 170 deaths were estimated in the US [1], while in 2011, 71 000 new cases and 8 700 deaths were estimated in France [2], making it the third most common cause of cancer death in men.

A number of treatment options are available, depending on a patient's age, medical history and anatomy, as well as on the stage of the cancer. The primary treatment options include: active surveillance without treatment, radical prostatectomy, chemotherapy, external beam radiation therapy (EBRT), and more recently, less invasive treatments such as cryotherapy, high intensity focused ultrasound (HIFU) and internal radiation therapy, namely brachytherapy. The latter method has, in recent years, increased in popularity among patients with early stages of cancer due to its low morbidity, short hospitalization and relatively few side-effects.

A. Permanent Low-Dose Rate Prostate Brachytherapy

Permanent low-dose rate (LDR) prostate brachytherapy is a technique that involves the localized irradiation of the prostate by the permanent insertion of about 100 tiny radioactive seeds. The conventional procedure introduces the seeds into the prostate according to a pre-operative dose distribution plan, by means of hollow needles inserted through the perineum of the patient in the lithotomy position. The number and distribution of seeds is determined to satisfy given dose constraints (in the prostate, rectum and urethra). A template, as seen in Figure 1, is used to insert the needles along a grid of horizontal holes, the depth of each needle being adjusted visually using two-dimensional trans-rectal ultrasound (TRUS) guidance. In our partner hospital, the technique takes between two and four hours under full anesthesia, depending on the complexity of each case. Its primary benefits over other popular techniques, such as radical prostatectomy and EBRT, are its short hospitalization period (1 to 2 days) as well as its potential for providing intense localized therapy within the prostate, with limited morbidity and side effects.

Recent discussions, motivated by the appearance of new studies showing a minimal death rate for early-stage prostate cancer patients [3], [4] have been provoked on whether treatments, including LDR prostate brachytherapy, are sufficiently beneficial to outweigh the side-effects and cost of the procedures. An important argument has been that the majority of the reported side-effects can be directly related to the quality and precision of the treatment delivered. The

This work was funded by the Agence Nationale de la Recherche (ANR) under the "Technologies pour la Santé" program (coordinated by Koelis SAS, La Tronche, France).

N. Hungr is with the Laboratoire TIMC-IMAG, Equipe GMCAO, 38706 La Tronche, France (phone: (+33) 4-56-52-00-09; fax: (+33) 4-56-52-00-55; e-mail: Nikolai.Hungr@imag.fr)

M. Baumann was with the Laboratoire TIMC-IMAG, Equipe GMCAO, Grenoble, France. He is now with Koelis SAS, 38700 La Tronche, France (e-mail: baumann@koelis.com).

J. A. Long is with the CHU de Grenoble, 38700 La Tronche, France. (e-mail: JALong@chu-grenoble.fr).

J. Troccaz is with the Laboratoire TIMC-IMAG, Equipe GMCAO, 38706 La Tronche, France (e-mail: Jocelyne.Troccaz@imag.fr). She is also with the CHU de Grenoble. She is funded by an INSERM CHRT grant obtained in 2010.

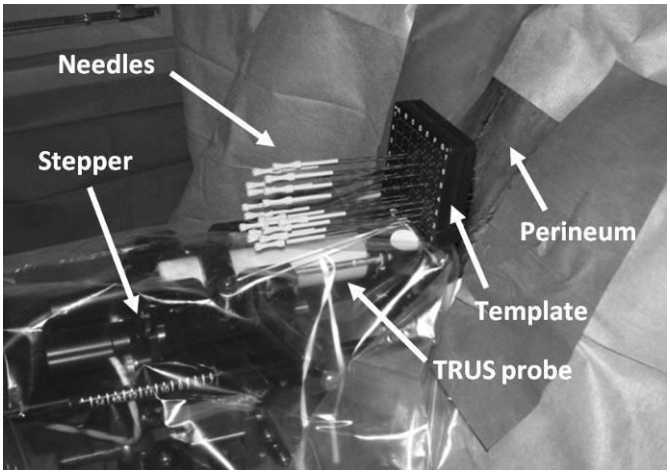

Fig. 1. Conventional brachytherapy setup in the OR.

success of a brachytherapy procedure (i.e. the complete destruction of the cancer, with minimal side-effects) is reliant on dose conformity, that is, the uniform distribution of the radioactive dose throughout the entire volume of the prostate (or the precise focalized application of the dose in the case of focal therapy), without overdosage and without affecting adjoining organs such as the bladder, rectum, seminal vesicles or urethra. The procedure is therefore heavily reliant on the ability of the clinicians and physicists in reproducing the pre-planned dosimetry within the prostate.

Multiple limitations to the conventional manual brachytherapy technique make dose conformity a difficult task. The primary challenge lies in the mobility of the prostate and surrounding soft tissues during the intervention. Both the insertion of the needles and the movement of the TRUS probe cause significant motion and deformation of the prostate [5], [6]. Since the dosimetry plan is typically based on the manual segmentation of only two sets of ultrasound images taken before the insertion of the needles (i.e. non-adaptive planning), the resultant accuracy of the seed placement is difficult to verify in real-time. This accuracy is additionally affected by a number of other factors, including the random migration of the seeds upon their release within the prostate, the flexion of the needles upon insertion into the tissue and prostatic edema during the intervention. Another important limitation to the technique is that needle insertion is restricted to the horizontal axes defined by the needle template. Not only is needle placement limited to a grid of 5mm spacing, but perhaps more importantly, this parallel grid system does not allow access behind the pubic arch in the relatively frequent case of the latter eclipsing parts of the prostate [7]. These issues, among others, result in a lengthy and unavoidably repetitive procedure that relies heavily on the experience of the clinicians and physicists and that limits patient eligibility.

B. Robotics in LDR Prostate Brachytherapy

Research in the field has, in recent years, turned towards using robotics and computer assistance with the primary goal of improving dose conformity. Numerous research teams worldwide have introduced novel conceptual advances towards the improvement of seed placement within the prostate. These advances are summarized in the columns of Table 1.

Robotics has introduced the possibility of positioning the needles throughout the prostate, without the grid constraints imposed by the template used in the conventional technique. Needle inclination is also possible, allowing to reach behind the pubic arch, thus potentially expanding procedure eligibility to patients with larger prostates.

Robotics can also be used to mitigate prostate motion and needle bending. During needle insertion, needle-tissue interactions cause significant motion of the prostate as well as needle flexion, making it difficult to reach the pre-planned seed locations with accuracy. This is managed in the conventional procedure by visually adjusting the depth of each needle based on the streaming 2D transrectal ultrasound (TRUS) images or by re-inserting the needle in case of large transverse errors. Due to significant image artifacts surrounding the needle, especially when multiple needles have already been inserted, this can often be more of an estimate than a precise adjustment. A mechanical approach for reducing prostate motion, made available by the use of robotics, has been to introduce controlled needle insertion speed coupled with needle rotation during insertion. This has been shown to decrease puncture force and deformation as well as needle deflection in phantoms [28], [29]. Another proposed solution has been the use of hooked stabilizing needles placed into the prostate [30], with however, the potential of causing increased bleeding and edema.

The other approach is motion management, rather than mitigation. By detecting the needles and/or seeds in the TRUS images [31]-[33], precise information can be provided to the clinician to help make informed decisions on how to proceed (whether this be needle re-positioning or modification of the planning). This detection also allows for automatic update of the dosimetry for post-operative evaluation. These techniques however, typically do not locate the needles and seeds with respect to the prostate and when used alone, cannot provide clinically relevant information on the dose distribution inside the gland. As in the manual technique, these detection methods are also often hampered by image artifacts, making them challenging in a clinical setting.

More recently, methods have been proposed for semi- or fully-automatically tracking the prostate itself in the ultrasound images [34], [35], [39]. One of these methods [39], developed previously by our group, will be described further in this article, showing its ability to track the prostate in near real-time and hence accurately manage prostate motion.

To date, all ultrasound-based robotic and manual techniques use 2D TRUS probes. Through the use of manual or motorized steppers, these 2D images can be reconstructed into three-dimensional (3D) volumes, on which the above-mentioned image analysis techniques can be used. In Table 1, we have called this method of 3D reconstruction "2.5D," in order to distinguish it from 3D probes that have moving elements

TABLE I
EXISTING ROBOTIC PROSTATE SYSTEMS AND THEIR INNOVATIONS

Primary Author	Year	Project Name	Status [a]	Ref	Imaging modality [b]	Unconstrained transverse needle positioning	Needle Inclination	Automatic needle insertion	Needle rotation	Multiple needle insertion	Automatic seed insertion	Automatic probe positioning	Rectal probe sleeve	Needle insertion approach [c]	Patient position [d]	Seed detection	Needle detection	Dynamic planning
Chinzei	2000		D	[8]	MRI	x	x							TP				
Fichtinger	2002		P	[9]	CT	x	x							TP	L			
Davies	2004		P	[10]	2.5D	x		x		x	x	x		TP	L	x	x	
Schneider	2004		P	[11]	2D	x						x	x	TR	L			
Phee	2005		C	[12]	2.5D	x	x	x				x		TP	L			
Wei	2005		P	[13]	2.5D	x	x					x		TP	L	x	x	x
Fichtinger	2006	PAKY	P	[14]	2.5D	x	x	x			x			TP	L	x	x	
Yu	2007	Euclidian	P	[15]	2.5D	x	x	x	x	x	x	x		TP	L	x		
Bassan	2007		P	[16]	2.5D	x	x	x	x		x	x		TP	L			
Podder	2007		D	[17]				x	x	x	x			TP	L			
Fischer	2008		P	[18]	MRI	x	x							TP	SD			
Patriciu	2007	MrBot	A	[19]	MRI	x	x	x			x			TP	LD			
Fichtinger	2008		C	[20]	2.5D	x	x							TP	L	x	x	
Salcudean	2008	Brachyguide	P	[21]	2.5D	x	x							TP	L			
Heikkilä	2008	NISE	P	[22]						x				TP	L			
Ho	2009	BioXbot	C	[23]	2.5D	x	x					x	x	TP	L			
van den Bosch	2010	UMCU	C	[24]	MRI	x	x	x						TP	SD			
Song	2010		P	[25]	MRI	x	x							TP	SD			
Bax	2011		P	[26]	2.5D	x	x					x		TP	L			
Krieger	2011	APT II	C	[27]	MRI	x	x							TR	PD			
Current paper		PROSPER	P		3D	x	x	x	x					TP	L			x

[a] D = Design stage, P = Phantom tests, A = Animal tests, C = Clinical tests.
[b] 2D = Two-dimensional ultrasound probe, 2.5D = Two-dimensional ultrasound probe with automated stepper, 3D = Three-dimensional ultrasound probe.
[c] TP = Trans-perineal, TR = Trans-rectal.
[d] L = Lithotomy position, LD = Lateral decubitus position, SD = Supine position, PD = Prone position.

within the probe-head itself. 2.5D techniques require probe movement within the patient's rectum which results in significant motion of the prostate due to the variable pressure applied to the rectum. Some research groups have elegantly countered this problem by developing fixed probe sleeves that ensure a constant pressure within the rectum (see Table 1). It is unclear, however, whether these sleeves affect image quality, especially at larger depths.

Another very different area of development has been the use of intra-operative MRI or CT scanners instead of US. These modalities can bring distinct information to the clinician that can be useful for more accurate anatomical segmentation or even focal cancer detection. The restricted space within these imagers requires the use of robotics in order to access the patient with ease and precision. These are very interesting but challenging initiatives that still require considerable development in order to gain the same confidence as the well-established US techniques.

C. Project Purpose and Justification

Advances in robotic-assisted brachytherapy research have clearly shown its potential in improving on the conventional manual techniques and providing benefits to patients and clinicians. The state of the art includes numerous creative designs for precise, efficient and robust robotic devices whose accuracy has been primarily validated on static phantoms. However, to be clinically beneficial, systems must couple the accuracy of a robot with techniques for managing the mobility of the soft tissue prostatic environment, in order to cope with the three situations illustrated in Figure 2: 1) motion and deformation caused by needle insertion, 2) needle bending and 3) deformation caused by TRUS probe motion. Mechanical solutions, such as introducing needle rotation, stabilizing needles, or probe sleeves can help reduce mobility, but are of limited utility as they cannot completely eliminate motion.

We believe, therefore, that a vital element for the clinical success of robotic brachytherapy systems is their ability to track the prostate in 3D space. In this paper we describe a novel robotic prostate brachytherapy system with prostate motion tracking. Our computer-assisted robotic brachytherapy system is called PROSPER (for PROState transPERineal interventions), and consists of a robotic needle insertion device, a static 3D ultrasound probe and a robust prostate tracking routine. The robot allows needles to be inserted throughout its continuous workspace (compared to the discretized template used in conventional brachytherapies), including at oblique angles, and at controlled insertion velocities and rotations. Unlike other systems, the 3D TRUS probe, calibrated to the needle insertion robot, allows for the

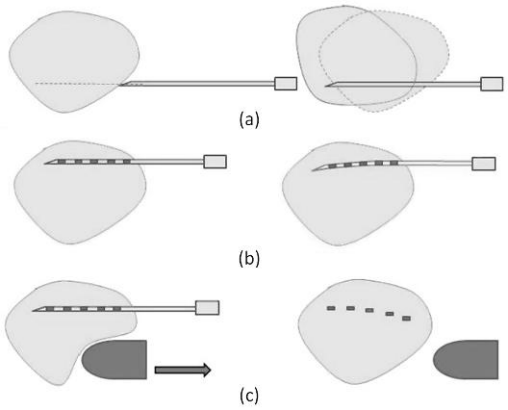

Fig. 2. Illustration of the three primary sources of prostate motion and deformation during brachytherapy. (a) Needle insertion causes a translation, rotation and deformation of the prostate. (b) A needle can bend during insertion, due to needle-tissue forces. (c) TRUS probe motion can cause prostate motion and deformation.

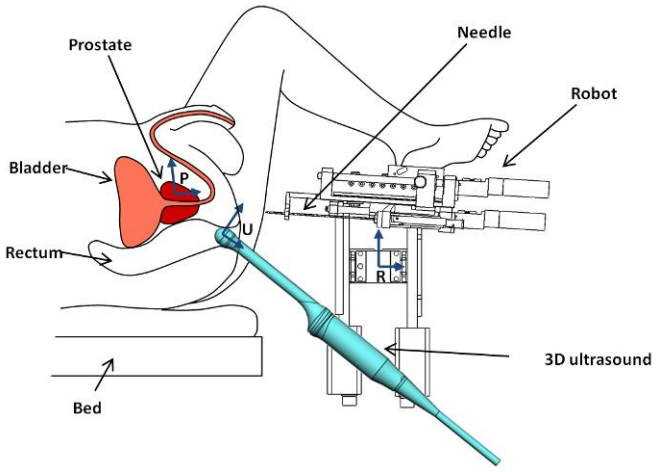

Fig. 3. Hardware layout within operating room. Reference frames: P = Prostate, U = Ultrasound probe, R = Robot.

automatic adjustment of needle depths based on gland motion detection during the procedure. In addition, the 3D probe remains stationary inside the rectum, preventing any probe-induced prostate motions. The clinical goal of the system is to improve the quality of the standard brachytherapy procedure by 1) ensuring a better correspondence between seed placement and the initial planned dose distribution, 2) providing a more diverse and flexible choice of seed positions in order to improve dose distribution and 3) potentially making the procedure available to more patients, particularly those with larger prostates or constrained pubic bone anatomies.

II. System Description

A. General Layout

The general layout of our robotic brachytherapy system is shown in Figure 3. As in the conventional technique, the patient lies on the surgical bed in the lithotomy position. The robotic needle manipulator is rigidly connected and calibrated pre-operatively to the 3D endfire US probe. At the beginning of the operation, the robot and probe are manipulated in unison by the clinician, by means of an adjustable fixation arm (such as the commercially available CIVCO Multi-Purpose Workstation) attached to the surgical bed, in order to place the probe in the rectum of the patient and obtain an appropriate visualization of the prostate. The whole assembly is then fixed and the 3D probe is able to acquire image volumes of the entire prostate without being displaced. It remains stationary for the entire procedure, unless the rectum-probe contact degrades due to patient motion, etc., in which case its position can be re-adjusted by the clinician. The robot adjusts its approach angle based on the orientation of the prostate gland in the US image. In analogy to the conventional stepper-based technique, the robot replaces the template in front of the perineum and the 3D probe replaces the 2D probe and stepper.

B. Clinical Workflow

The clinical workflow that we have designed for our system is illustrated in the block diagram of Figure 4. At the beginning of the procedure, a 3D US reference volume is acquired. It is registered to a pre-operative MRI acquisition to facilitate and improve prostate delineation [36] and initial dose planning [37]. In this initial planning stage, the needle trajectories and seed positions are defined with respect to the reference prostate extracted from the US reference volume.

Next, the following process takes place for each needle. The needle trajectory is computed with respect to the robot coordinates by means of a pre-operative calibration of the US probe with respect to the robot. The robot positions the needle at its insertion point in front of the perineum and inserts the needle. In case of pubic arch interference, the needle is withdrawn and a partial re-planning is done to modify the needle trajectory in order to avoid the pubic arch, while still maintaining the dose constraints. Once the needle has been inserted to its planned position, a verification procedure is applied to check for and respond to any prostate motion or deformation caused by the insertion.

The control loop used to handle prostate motion is highlighted by the gray background in Figure 4. It is important to note that in our control scheme, the dosimetry plan is fixed with respect to the mobile prostate reference frame, rather than to the stationary US probe as is the case in the conventional procedure (see frame P in Figure 3). By taking a US volume after the needle insertion, and registering it to the initial reference volume, the dosimetry plan can be deformed in conformance to the prostate's motion and deformation. If the needle's target has moved during insertion, we first check if it can still be reached following the same needle trajectory. If it can be reached, the needle depth is adjusted iteratively until the clinician is satisfied with the proximity, as shown in Figure 5. Otherwise, if the clinician deems the current needle location as unacceptable, the needle is withdrawn and a partial re-planning is done in order to compensate for prostate motion before re-inserting the needle. This re-planning can be done using the clinician's experience to offset the needle's insertion point accordingly, as is currently done in conventional

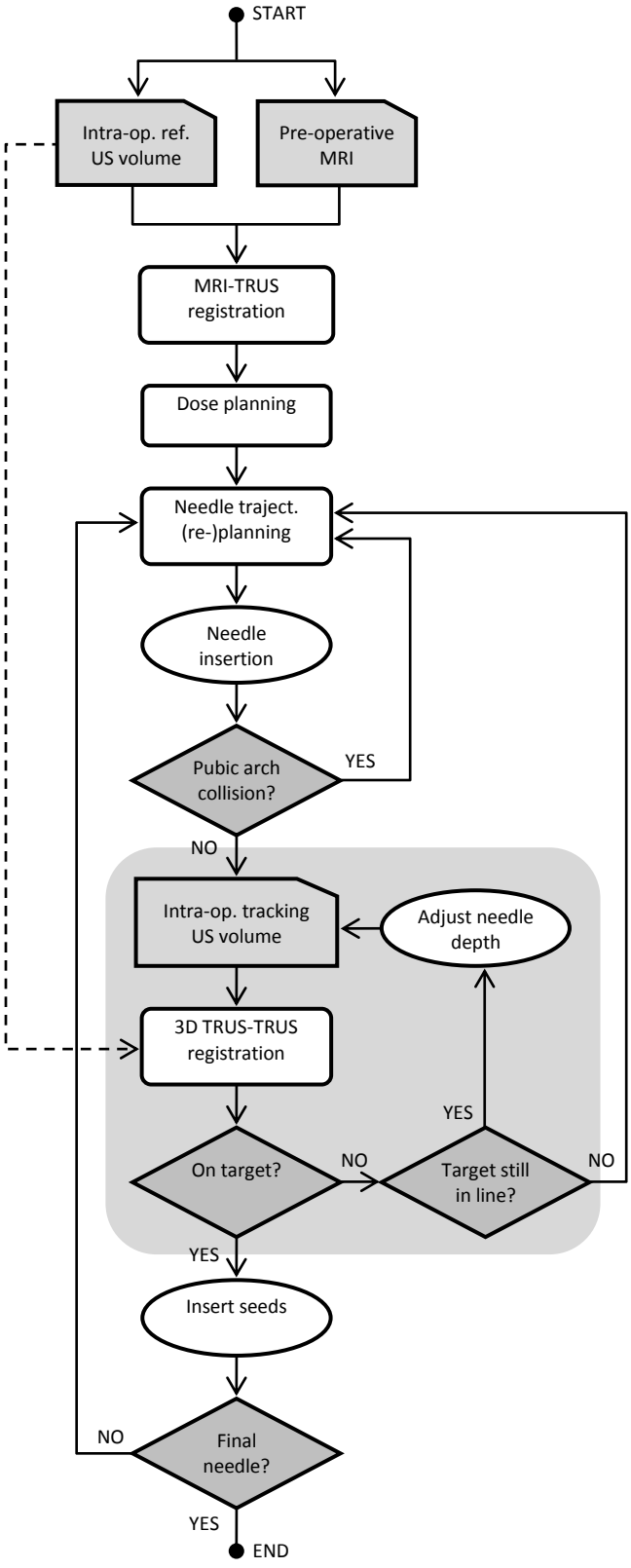

Figure 4: Block diagram illustrating the clinical workflow that we propose for our system.

brachytherapies.

Once the clinician is satisfied with the final needle position, the seeds are inserted (with the « Mick Applicator » for instance) while progressively removing the needle. A 3D US volume may be acquired for checking the position of each seed separately or globally for all the seeds of a needle. This procedure is repeated until all seeds have been distributed in the prostate.

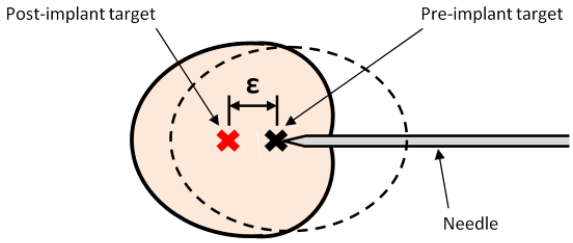

Fig. 5. Simplified illustration of how the prostate deforms during needle insertion, moving the pre-implant target within the deformed prostate. The pre-implant prostate shape is depicted by the dashed circle. Our system registers the pre-implant image to the post-implant image and determines the amount ε by which the target has moved, allowing this to be corrected by advancing the needle further.

III. Prototype Description

A laboratory prototype was built to evaluate the system's performance in a synthetic, deformable prostate phantom environment. The aspect of the clinical workflow that was tested with this prototype, was the grey motion-compensation loop shown in Figure 4, in which US-US image registration is used to determine the motion and deformation of the prostate in order to correct the needle insertion depth. The layout of the prototype system is shown in Figure 6(a) and consists of a robotic needle manipulator connected to a rigid table-mount stand, onto which is also rigidly fixed the 3D ultrasound probe. A rigid stand was used rather than an adjustable fixation arm (as described in Section II.A) for manufacturing simplicity. The robot is controlled by a laptop through a serial RS-232 connection, while the ultrasound probe is controlled by an ultrasound machine. A synthetic prostate phantom used during our tests can also be seen in Figure 6(a).

In this section, we will describe the various components of our prototype system in detail, before moving on to a description of our tests.

A. Robotic Needle Manipulator

The prototype robotic needle manipulator used to position and insert the needle according to the procedure defined by our control scheme has been described in a previous publication [38]. A photograph of the prototype is shown in Figure 6(b). It consists of two primary elements: a 5 degree of freedom (DOF) needle positioning module and a 2 DOF needle insertion module. The positioning module positions the needle along the appropriate insertion axis, allowing needle inclinations in the sagittal and coronal planes. The insertion module drives the needle to a given depth and can rotate the needle during insertion if necessary. The clinician inserts the seed manually.

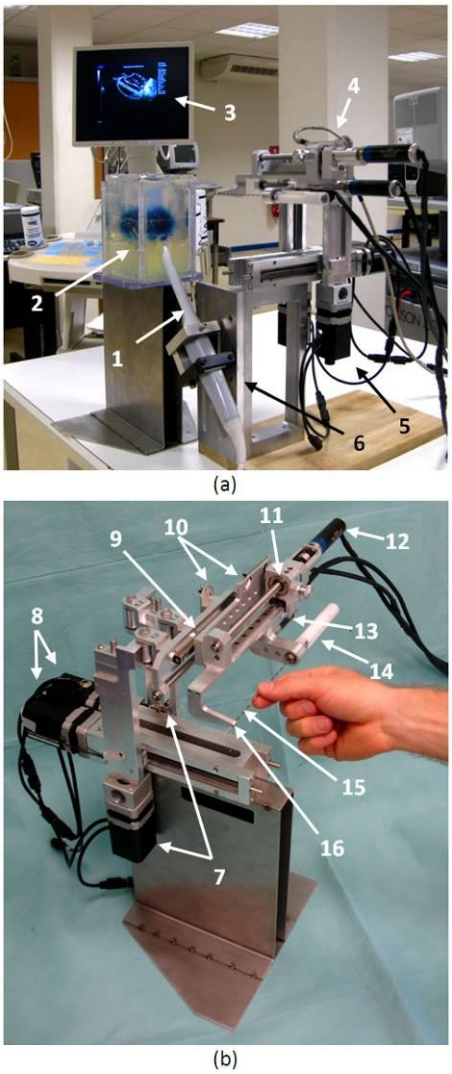

Fig. 6. (a) Test-bench setup showing all the components of our system (1: 3D endfire US probe, 2: prostate phantom, 3: US machine, 4: needle insertion module, 5: needle positioning module, 6: laboratory robot-probe stand). (b) Photograph of our first robot prototype (7: vertical motors, 8: horizontal motors, 9: Z-translation motor, 10: homing Hall sensors, 11: needle disengagement mechanism, 12: needle insertion motor, 13: needle rotation motor, 14: needle grip, 15: needle, 16: needle guide / robot end effector).

The prototype's workspace is defined by 105 mm of horizontal and vertical translation in the transverse plane, 90 mm of translation in the cranial-caudal direction (i.e. in the direction of the needle) and 30° of inclination in the sagittal and coronal planes. In comparison, a conventional brachytherapy needle template has a workspace of 60 by 60 mm in the transverse plane, with needle holes every 5 mm and no possibility of inclination.

The needle insertion module allows for a maximum needle insertion depth of 105 mm along with the possibility of rotating the needle at up to 12 rotations per second (rps). A mechanical release system that disengages the needle driver at a needle force of around 20 N, in case of needle-bone contact, prevents the patient from being harmed and the needle from breaking. It also allows for manual retraction of the needle in case of an electronics malfunction. The needle grip shown in Figure 6(b) is manually releasable in order to rapidly plug a Mick Applicator or other type of seed dispenser onto the needle head. Details of these features can be found in [38].

B. Robot Sterilization

The inclusion of robotic tools in the operating room always introduces the challenge of sterilization compatibility. Since our robot uses motors and complex moving parts (bearings, ball-screws, linear rails, etc.), we are unable to place it entirely in an autoclave. Other methods of sterilization (such as hydrogen peroxide and radiation) were discarded due to size and availability issues.

Sterilization was, therefore, resolved as shown in Figure 7. The needle guide (see Figure 6(b)) at the front of the needle insertion module is sterilizable and exchangeable to accommodate different diameter needles (ex. 18G or 17G). The rest of the needle guide is cleaned but not sterilized. Instead, it is covered by a sterile plastic cap that prevents any non-sterile parts from accidentally touching the sterile zone. The needle itself is fastened to the rotation hub by a removable, sterilizable plastic bushing that provides the interface between the sterile needle and the non-sterile elements of the robot (Figure 7(b)). The positioning module is covered by sterile drapes, as is done with the stepper in the conventional procedure (see Figure 1).

C. Ultrasound Machine and 3D Probe

The 3D TRUS probe is a crucial element of the PROSPER system. A 3D probe consists of a 2D array of US transducers

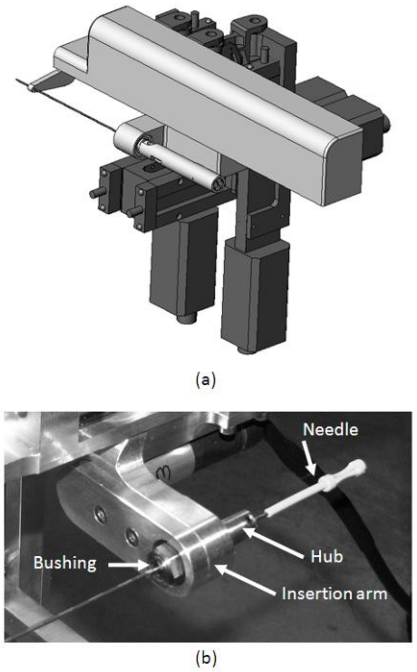

Fig. 7. (a) CAD model showing how the needle insertion module can be covered by a sterile plastic cap. All white parts are sterile, while all black parts are covered by a sterile drape. (b) Detail of the needle insertion arm, showing the location of the sterile bushing that separates the sterile needle from the non-sterile rotation hub.

mounted to a miniature motor hidden inside the probe head,

compared to stepper-based 3D acquisition systems which use a 2D probe mounted on a manual or automatic stepper that moves the entire probe during acquisition. Our 3D probe, once inserted into the patient's rectum, remains stationary for all volume acquisitions, eliminating probe-induced movements of the prostate. It is also faster and allows for more precise volume acquisition.

Two types of probes could be used: an axial side-fire probe or an end-fire probe, each providing certain benefits over the other. A side-fire probe would provide image views similar to those clinicians are accustomed to seeing with conventional bi-plane TRUS probes. In addition to acquiring 3D volumes, it could also allow for real-time 2D viewing of needles parallel to the probe axis. An end-fire probe would have to be inserted at a steep angle, as shown in Figure 3. This angled approach presents the advantage of allowing more space for needle inclination; however the presentation of familiarly oriented 2D slices requires more complex image reconstruction.

At the time of construction of our prototype system, no side-fire probe was available, so an Ultrasonix 4DEC9-5 end-fire probe was used and connected to an Ultrasonix RP ultrasound machine. The 10 MHz probe has 128 elements arranged in a convex line, allowing for 145 degrees of coverage between end elements and 106 degrees of sweep. The Ultrasonix RP was chosen for its research interface that allows for full control of low-level probe parameters and image reconstruction directly on the machine.

We developed a user interface for imaging 3D volumes with the Ultrasonix probe. The interface is shown in Figure 8. It allows the user to acquire 3D volumes and display them in a Cartesian reconstruction. The user can scroll through sagittal, transverse and coronal views (with respect to the probe's long axis). The speed of sound used in the reconstruction can be set, allowing for geometrically correct imaging in different mediums. The interface also allows pairs of images to be registered together. Points can be specified in the images and used as needle targets for the robot. Image registration determines the image deformation field and applies it to the point locations as well. The ultrasound interface is connected to the robot control laptop by a network cable, allowing target points to be sent directly to the robot.

D. *Image Registration*

The non-rigid image registration algorithm used in the PROSPER system was developed in our laboratory in the context of prostate biopsies for the computation of 3D maps of prostate biopsies on a reference volume in presence of motion and deformation; it has been described in the literature a number of times already [39]-[42]. It is fully automated and solely based on the analysis of image-intensity variations, i.e. it does not rely on the explicit identification of prostatic structures. The algorithm uses a multi-step pipeline, where each step refines the registration on increasingly more complex motion models. Rigid registration steps are performed using the correlation coefficient as similarity measure. Deformation estimation is carried out using a variational approach with linear elasticity as motion constraint. Additionally, for two volumes I1 and I2, the forward transformation (mapping I1 to I2) and the backward transformation (mapping I2 to I1) are estimated simultaneously and connected via an inverse consistency constraint to improve the registration behavior in the presence of noise. A novel similarity measure that we call 'shift correlation' is used for very fast yet precise ultrasound to ultrasound registrations. The registration has been validated on 47 biopsy patients and 786 registrations using segmented fiducials inside the prostate as ground truth for accuracy evaluation. The RMS error of the system was evaluated to 0.76±0.52 mm, and the time required for a single registration was about 6-8 seconds on a 2.4 Ghz Intel Core 2 standard PC.

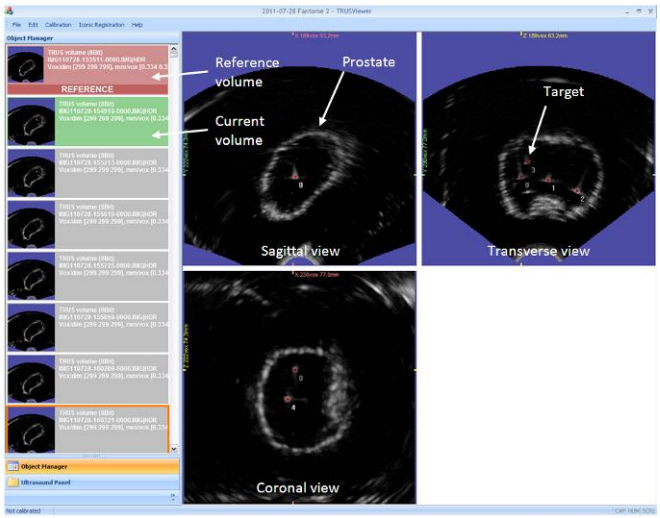

Fig. 8. User interfaced for image acquisition with the Ultrasonix 3D probe.

IV. Calibration

The accuracy of the PROSPER system relies in part on the mechanical relationship between the rigidly connected robotic needle manipulator and ultrasound probe. Calibration is therefore an important step. Two calibrations were performed: a calibration of the robot kinematics, followed by a calibration between the 3D US image space and the robot space.

A. *Robot Kinematics Calibration*

The robot kinematics was calibrated in order to improve the kinematic accuracy of the robot, initially based on the 3D CAD model of the prototype. More specifically, the robot's Denavit-Hartenberg (DH) parameters (see Appendix) were calibrated based on measurements of the robot's end effector in various poses throughout its workspace. A Polaris optical measurement system (Northern Digital Inc.) was used to measure the poses. Although the reported accuracy of the Polaris system is not ideal (0.25 mm) for the high precisions required for such a medical application, it was chosen for availability and simplicity reasons, and deemed sufficient for the laboratory use of this first prototype.

The transformations between the various reference frames used in the kinematic calibration are shown in Figure 9. Two Polaris rigid bodies were used, one attached to the base frame

of the robot, and the other to its end effector. Note that the robot end effector refers to the pin hole at the end of the robot, through which the needle passes, as labeled in Figure 6(b). The transformations between each rigid body and the true robot base/end effector were estimated and added to the list of unknown parameters to solve for in the calibration routine. 48 different poses were measured throughout the robot's 3D workspace and at random horizontal and vertical inclinations, giving a system of k = 48 equations and 14 unknown robot parameters (8 DH parameters and 6 motor offset parameters) as follows:

$$\varepsilon_k = {}^{pol}_{k}x_b^{ee} - {}^{fkin}_{k}x_b^{ee}(P, q_k) \quad (1)$$

where ε_k is the error between the pose from robot base to end effector measured by the Polaris (${}^{pol}_{k}x_b^{ee}$), and the pose calculated by the robot forward kinematics (${}^{fkin}_{k}x_b^{ee}$). P is the set of DH parameters being solved for, while q_k is the set of robot joint positions at each pose k. The pose measured by the Polaris is derived from the following transformation relationship:

$${}^{pol}_{k}T_b^{ee} = T_{RBb}^{b\ -1} \times T_{pol}^{RBb\ -1} \times T_{pol}^{RBee} \times T_{ee}^{RBee\ -1} \quad (2)$$

where the various transformations can be seen in Figure 9. The error in (1) was minimized using the least squares Levenberg–Marquardt algorithm. Table 2 shows the values of robot's kinematic parameters before and after the calibration.

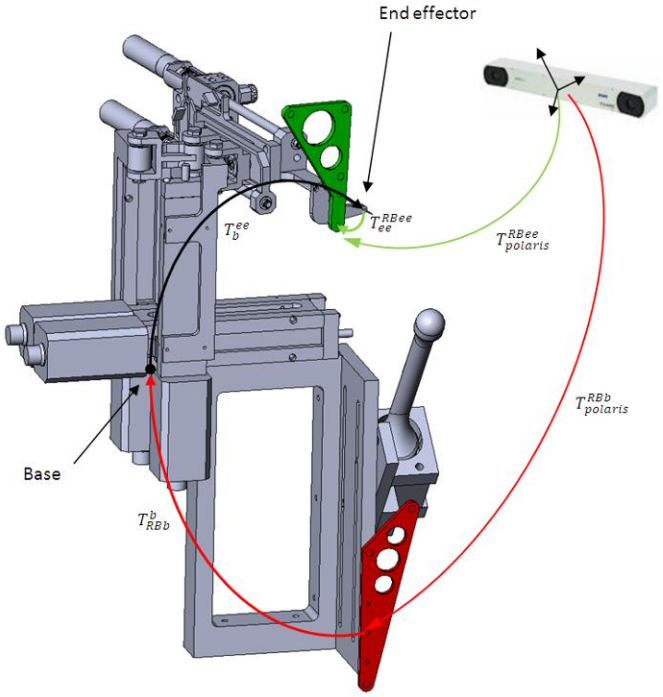

Fig. 9. Transformations used between the various reference frames during kinematic calibration of the robot. RB = rigid body, b = robot base, ee = robot end effector (for example, T_b^{ee} = transformation between robot base and end effector).

TABLE II
KINEMATIC PARAMETERS BEFORE AND AFTER CALIBRATION

	Before	After
DH Parameters		
D0	-0.9	-0.903
D4 and D11	109	109.000
A4 and A12	35	34.997
(D0 + D7)	-41.3	-41.297
A10	45	45.021
D12	38	38.015
Motor Offsets		
M1	48.205	48.184
M2	5.015	5.036
M3	164.42	164.436
M4	165.5	165.483
M5	25.75	25.753
M6	17.95	17.950

All values in mm.

With the new parameters, the average error between the calculated and measured poses was decreased by over a half to 0.5 mm, just above the accuracy of the Polaris.

In this calibration routine, the needle tip was not calibrated due to the technical challenge of measuring the tip of the thin, flexible needle. The tip accuracy at various depths was, however, tested after calibration, by inserting patterns of holes in a flat vertical foam board mounted in front of the robot (Figure 10). The patterns were digitized and the distances between respective holes measured to determine the positioning error at the needle tip. The results showed that needle insertion added about 0.1 mm to the calibration error. This error likely increases during insertion into actual material, where needle-tissue interaction forces may cause needle bending.

B. Robot-US Probe Calibration

The calibration between the robot space and the image space enables the target points in the image to be transformed into robot coordinates in order to send the robot to the corresponding point in space. Since the probe and robot are rigidly fixed together, this calibration is necessary only once, after which the system stays calibrated, provided the probe is kept in place or is installed on the robot before each procedure in a repeatable manner (through the use of a keyed connection, for example). This calibration is vital in defining the accuracy of the system.

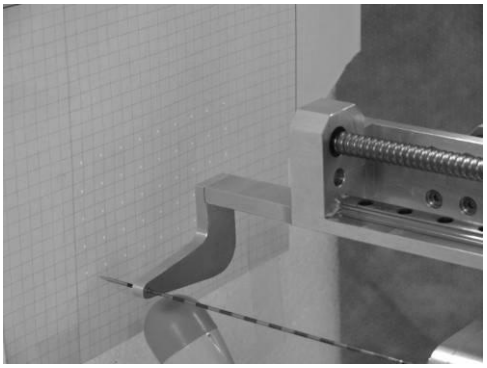

Fig. 10. Setup used to test needle insertion accuracy after kinematic calibration. The pattern of holes used to measure this accuracy can be seen on the gridded paper in front of the needle.

The method we used for this calibration was to insert the needle into a water bath at a number of different poses, segmenting the needle tip in the US image and then registering the two point clouds (one in robot space and one in image space) together to find the best-fit transformation between them. Although the method is simple and commonly used, it was in fact challenging to segment the needle in the water in a reliable and repeatable manner. As can be seen in Figure 11(a), the US image of the needle was subject to 1) intense reverberation artifacts when the needle was tangent to the probe head surface and 2) a decrease in resolution at larger distances from the probe head (for deep or high needles). This resulted in a needle tip that was typically very difficult to distinguish, with a segmentation repeatability of greater than 2 to 3 mm, even with semi-automated segmentation algorithms. To improve the localization of the needle tips in the images during calibration in water, we constructed a small rubber sleeve with a soft ball at one end. Once placed on the needle tip, the ball was very visible in the image, while the rubber sleeve diminished the reverberation artifacts, dramatically improving segmentation quality.

To prevent any adverse gravitational effects on the kinematics of the robot, we calibrated the robot in its normal horizontal position, instead of tipping it vertically above a water bath, as is typically done in such calibrations [20], [26]. For this, we developed the calibration basin shown in Figure 11(d). It is placed in front of the robot, like the phantom shown in Figure 6(b). A thin, soft PVC membrane was fabricated and placed on the front of the basin, allowing the needle to pierce through into the water behind without bending, while preventing water from leaking after withdrawal of the needle (note that the rubber sleeve described in the previous paragraph was placed on the needle tip only once the needle had pierced this membrane and entered into the water). An orifice was made at the base of the membrane, through which the US probe was inserted and sealed to prevent water leakage. The basin was filled with water at room temperature. The water's temperature was measured precisely and used to adjust the speed of sound used in the US image reconstructions, using the Bilaniuk and Wong equation [43].

Two separate calibrations were done, with 25 robot poses each, covering the entire robot workspace and needle insertion depths. The ball-sleeve was manually segmented in the images at high zoom after each insertion. The cloud of segmented points was then rigidly registered to the corresponding points stored in robot space using Arun least squares fitting [44]. The resulting registration errors are shown in Table 3 and are consistent for both calibrations. 10% outlier elimination was used to eliminate major outliers caused by manual segmentation error in points typically very deep and far from the probe head. The calibration errors were less than 1 mm, which was satisfactory given the repeatability of the manual segmentation, the 0.33 mm^3 resolution of the images and the kinematic calibration error mentioned in the previous section.

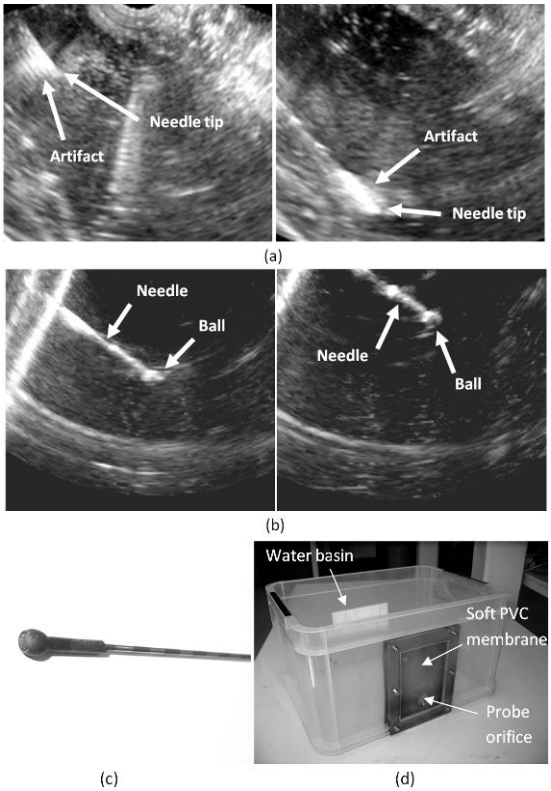

Fig. 11. (a) Example US images showing the artifacts present with a bare needle in water. (b) Images showing improved visibility by placing a rubber sleeve over the needle tip. (c) Photograph of the rubber sleeve and ball placed over the needle tip. (d) Calibration basin designed to calibrate the PROSPER system in the horizontal position.

TABLE III
ROBOT-US PROBE CALIBRATION ERRORS

Calibration	# of points segmented	All points		Outlier elimination	
		RMS error	Max. error	RMS error	Max. error
1	25	1.04	1.84	0.86	1.32
2	25	1.07	1.78	0.92	1.34

All values in mm.

V. PHANTOM TESTS

We conducted phantom experiments on our system to examine its efficacy and accuracy. We performed a set of simulated brachytherapies on anthropomorphic synthetic prostate phantoms that we developed in our laboratory. The results were measured by segmenting the inserted seeds in CT scan volumes of the phantoms.

A. Phantom Description

In order to test our system's ability to handle prostate motion, we had to develop a realistic phantom. Not only was realism required in the US images of the phantom, but also in the mechanical soft-tissue behavior of the phantom prostate during needle insertion. Our prostate phantom is shown in Figure 12. It was made of soft PVC plastic of varying softness. The relatively rigid prostate was enveloped in a thin coating of echogenicity-enhanced PVC (blue coloring) and embedded in a much softer medium which was, in turn, set within a more

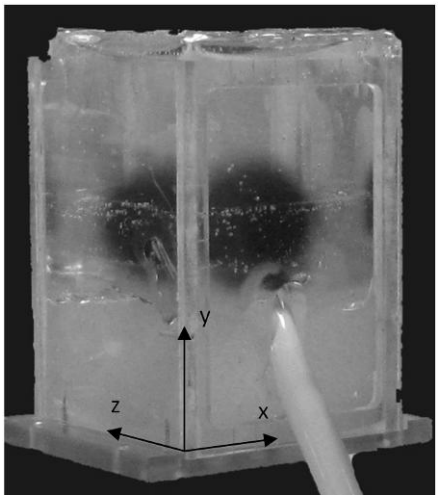

Fig. 12. Photograph of the custom prostate phantom used in our tests.

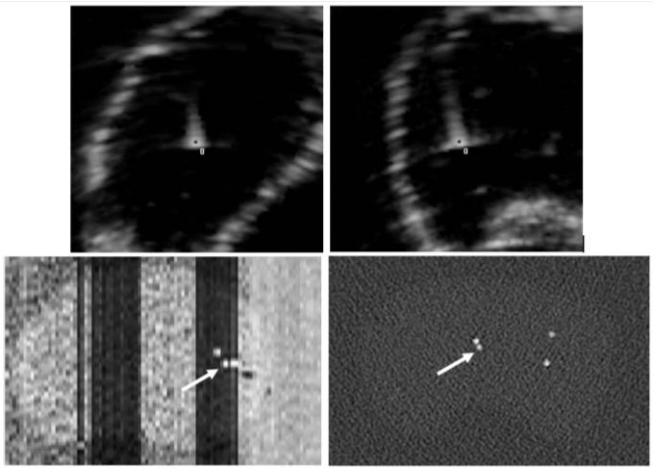

Fig. 13. sagittal (left) and transverse (right) cuts of a US volume (top) and a CT volume (bottom) acquisition of the prostate phantom, showing the prostate outline, target beads and inserted beads (marked by arrows in the CT images). Note in the sagittal CT view, the two inserted beads in line: the second bead being used to distinguish between inserted and target beads.

rigid outer container that represented the perineum. The latter structure had a concave hole below the perineal wall, representing the rectum. The phantom was placed in a rigid Plexiglas frame, with the perineum side exposed. The prostate was molded with a dozen 1 mm diameter glass beads embedded inside, acting as targets for needle insertion. The beads were embedded in two layers: 6 beads in a shallow layer near the apex of the prostate, and 6 beads in a deep layer near the base.

The US probe was inserted into the phantom's rectum, giving fairly realistic images of the prostate, with the glass targets being very easily segmented. Needle insertion into the phantom resulted in noticeable prostate motion of up to 7 mm in translation and around 2 degrees in rotation (in both transverse and sagittal planes). In vivo motion, reported in the literature, has mentioned similar motions on the order of 3-10 mm of translation [5] and slightly larger rotations ranging between 0 and about 10 degrees [6]. The phantom and its targets could also be seen clearly in CT images, allowing us to verify seed placement in CT volumes. The detailed manufacturing and behavioral features of this phantom have been published in [45].

B. Test Description

The experiment conducted with the PROSPER system involved trying to insert seeds as close as possible to the glass targets embedded in the phantom prostates, using the control loop described above in Figure 4. The goal of the experiments was to determine how well the system was able to handle prostate motion and deformation and with what accuracy. Nine phantoms were constructed, each with 12 target beads embedded inside, giving 108 targets in total.

After a first reference volume acquisition, the target beads in the phantom were located by hand at high zoom (at least 3x zoom), as shown in Figure 13. Using the first robot-probe calibration result in Table 3, the target coordinates were sent to the robot, which proceeded to insert the needle accordingly. An 18 gauge Mick Ripple-Hub needle (Mick Radio-Nuclear Instruments, Inc.) was used, with an insertion speed of 5 mm/s and a rotation speed of 8rps. The rotation speed was chosen based on experiments done on the soft PVC used in the phantom which showed that an increasing rotation speed decreased the needle insertion force up to 8 rps, beyond which the force did not vary significantly (at least up to the speeds available with our prototype). Once the needle was inserted, a second volume was acquired and the initial reference volume was registered to it. The deformation field was applied to the original segmented target location, and the new deformed target location was sent back to the robot. The robot then adjusted the needle depth to the closest point along the needle axis to this new target location. This was repeated until no further depth change could be made.

Once the needle was in place, the needle stylet was removed and a 1 mm diameter glass bead was inserted using a second stylet with its tip cut off, allowing the bead to be dropped exactly at the end of the needle cannula. To be able to distinguish the inserted bead from the target bead, the needle was then retracted a few millimeters, and a second bead was deposited in line with the first, acting as a marker for the CT images (see Figure 13).

Targets that were near the superior surface of the prostate were approached at a 10˚ horizontal and vertical inclination to simulate pubic arch avoidance. All the other targets were approached in a horizontal, cranial-caudal direction, as in the conventional template-based brachytherapy technique.

The phantoms were then imaged in a Philips Brilliance 64 clinical CT scanner at a scanning resolution of 0.15 x 0.15 mm per pixel and 0.33 mm slice spacing. The target beads and inserted beads were segmented by hand, at high zoom in each phantom, and the distance between them was measured. During needle insertion, the total amount by which the robot corrected the needle depth after registration was recorded as well.

C. Results

The results of the experiment are shown in Table 4. The measurements done on each target are explained in Figure 14. Of the 108 target beads available for insertion, half were near the apex of the prostate, while the other half were near the base. Some target beads, primarily at the base of the prostate, were difficult to segment reliably and were consequently discarded, resulting in 50 measurements at the apex and 40 at the base.

The average amount by which the needle depth was corrected after image registration, in order to correct for prostate motion, was 4.36 mm for needles inserted at the apex and 6.94 mm at the base of the prostate. The average Euclidean distance between the centers of the target and inserted beads was 2.28 mm at the apex, while at the base it was 3.86 mm. The distance between beads in the horizontal cranial-caudal depth direction (i.e. in the needle insertion direction) for the horizontal insertions was 1.43 mm at the apex and 1.98 mm at the base. The latter results show that the effect of prostate motion on insertion accuracy was improved by about 75% in the needle direction for both apex and base insertions. The accuracy of angled needles compared to horizontal needles was not significantly different, although the former tended to be about 5-10% more accurate.

A large majority of the targets required only one single depth correction to reach the final insertion point, while about 5% required two or more corrections.

Timewise, an entire bead insertion, with one depth correction and two image acquisitions and registrations, took less than 3 minutes. Acquisition of the image volume by the 3D Ultrasonix probe took 17 seconds, while registration took 7 seconds (on the 40 MHz, 1.0 GB of RAM Ultrasonix RP system, running Windows XP Professional).

VI. Preliminary Cadaver Feasibility Study

The goal of the experimentation on synthetic phantoms described in the previous section, was to show the effectiveness of the PROSPER system in managing prostate motions in a simplified environment. The next stage will be to assess the system in a more realistic and complex situation. We have therefore done a preliminary feasibility study on a cadaver to determine whether 1) we are able to acquire realistic US images (as little proof of this was found in the literature), 2) our registration algorithm works on these images, 3) the cadaveric prostate is mobile upon insertion of a needle and 4) our system is ergonomically feasible on a patient in the lithotomic position.

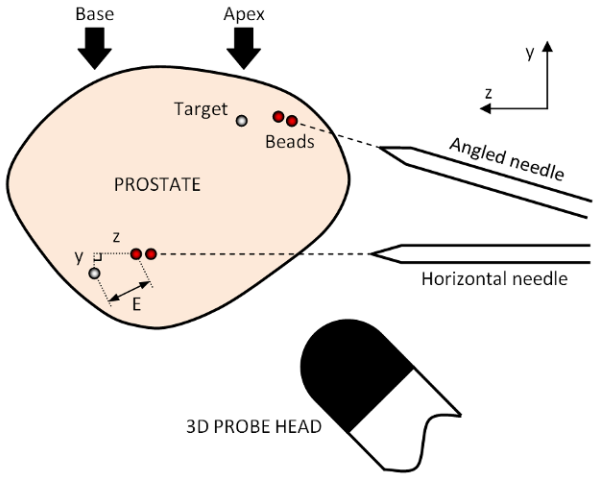

Fig. 14. Illustration of the measurements done during phantom testing. E stands for Euclidean distance. The x-direction comes out of the page and is not shown in the illustration.

An embalmed cadaver with an intact prostate, measuring on the order of 25 cm^3 was used. The specimen was mounted on the operating table in the lithotomic position and the robot-probe combination put into place in the rectum, as seen in Figure 15(a). The robot was easy to place and did not interfere with the raised legs of the specimen. Access to the operating site was minimally obstructed by the presence of the robot, as it was hidden under the specimen's left leg. The robot workspace was sufficient to reach all necessary parts of the perineal area.

The images obtained were very realistic compared to real in vivo images (Figure 15(b)). To test the registration algorithm, a reference volume was taken, followed by a second image after moving the probe manually inside the rectum. Image registration of the two images was successfully achieved, as shown in Figure 15(b). During cadaver manipulation, it was evident that the cadaver tissue was significantly fixed by the formaldehyde used during embalming, making the prostate and surrounding tissues very rigid. Manual needle insertion, although similar in feel to in vivo needle insertion, resulted in very little, if any, prostate motion. Motion, in fact, was limited to localized deformations around the needle, rather than global prostate motions.

TABLE IV
Phantom Experiment Results

Location	# beads	Distance between target and inserted (mm)				Depth correction (mm)
		Euclidean	x	y	z	
Apex	50	2.28 (0.73)	1.15 (0.77)	0.94 (0.66)	1.37 (0.79)	4.36 (1.73)
Horiz.	35	2.32 (0.64)			1.43 (0.80)	
Angled	15	2.19 (0.91)				
Base	40	3.86 (1.27)	2.40 (1.72)	1.52 (0.96)	1.91 (1.00)	6.94 (1.71)
Horiz.	32	3.92 (1.34)			1.98 (0.98)	
Angled	8	3.60 (0.99)				

Values in parentheses represent standard deviations. The x and y axes are, respectively, the horizontal and vertical directions in the transverse plane, while z is in the horizontal cranio-caudal depth direction, as shown in Figure 13.

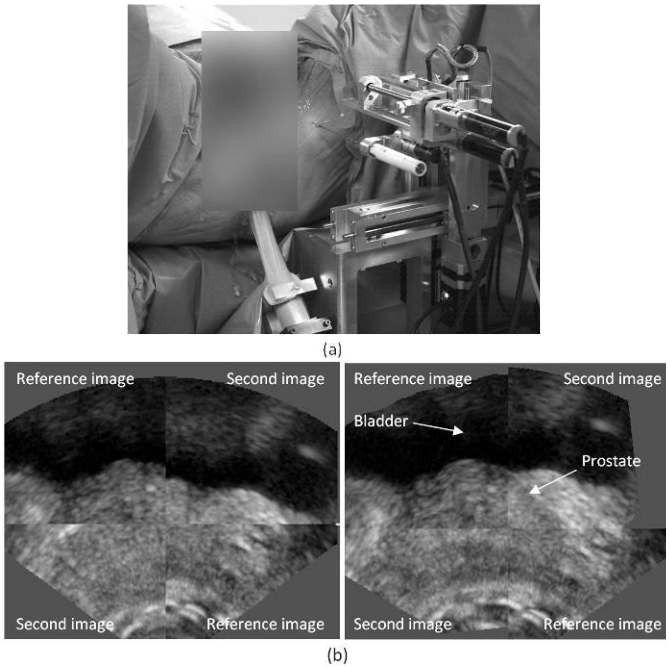

Fig. 15. (a) The prototype PROSPER system in place during the cadaver study. (b) Transverse view of two ultrasound volumes overlain on top of each other before registration (left image) and after registration (right image).

Robotic needle insertion was also tested. An important finding was that needle rotation, using a triangular-tip, 18 gauge Mick Ripple-Hub needle, at any rotation speed, caused the cadaveric tissue to wrap around the needle and completely seize it in place. This not only made it impossible to insert the needle, but also caused permanent tissue damage, visible as white artifacts in the image. Further study would be required to determine whether this behavior was characteristic of the cadaveric tissue or of the needle type. Needle insertion without rotation was effective, however, it was evident that the speed of sound was not 1540 m/s (as used in standard ultrasound machines), as the needles did not by any means reach the target points selected on the reference image. Another drawback was that needle insertions tended to progressively damage the prostate, resulting in a deterioration of the image quality due to white artifacts.

Although no quantitative data has been achieved with this preliminary cadaver test, we think the observations described in this section could be of use to researchers who may be envisioning similar tests. We plan on furthering these tests on fresh cadaver specimens.

VII. Discussion

The purpose of the phantom experiment described in section V was to determine how well the PROSPER system was able to compensate for prostate motions and deformations due to needle insertion. The results show that in our synthetic phantoms, needle insertion caused significant motion, on the order of 4 to 7 mm. Without the registration step, the resulting seed distribution would have been significantly offset from the planned distribution. By correcting the needle depth based on the prostate motion, the accuracy of the system in the needle insertion direction was less than 2 mm, which is an encouraging result, given it includes non-negligible measurement errors and errors inherent to the experiment itself, as we will describe in the following paragraphs. This accuracy compares favorably to other proposed computer-assisted brachytherapy systems in the literature: [26] report an error of 1.6 mm for their system, [13] report an error of 0.79 mm, [16] report an error of 1.45 mm, [20] report 1.04 mm, [23] report <1 mm, [21] report 1.22 mm and [15] report 0.69 mm. All of these reported values were measured on static, non-deformable phantoms, so our result is especially encouraging, as it includes prostate motion.

One error comes from the initial segmentation of the target beads in the reference US images. The amount of error attributed to this manual segmentation is difficult to quantify, however, the high zoom used during segmentation could allow us to estimate an error on the order of a voxel width or two, in addition to the error attributed to the image resolution itself ($0.33\ mm^3$), resulting in a root sum of squares (RSS) error of 0.47 mm. This error means the initial target position sent to the robot was already inaccurate. Afterwards, once the result was obtained, in the form of the CT image, a similar manual segmentation error was also present (0.47 mm as well). The total RSS segmentation error affecting the accuracy measurements could therefore, be estimated at 0.66 mm.

Another source of error that affected the results was the speed of sound used in the reconstruction of the US images, which was found to be 1380 ± 20 mm/s. This variability in speed of sound would cause an error of ±1.5% of the target's distance from the probe head. For the shallowest targets (~20 mm from the probe head), this would amount to about 0.3 mm, while for the deepest targets (~60mm), the error could be up to 0.9 mm.

Combining the two sources of error described above, would result in a RSS measurement error of up to 1.1 mm, which significantly improves the actual system accuracy.

The sources of error intrinsic to the PROSPER system itself, excluding the measurement errors, include the kinematic (0.5 mm) and robot-probe calibration (0.86 mm) errors described above, as well as the US-US image registration error (0.76 mm). Combining these would give an RSS error of 1.3 mm, which approaches the accuracy measured during the experiments.

The essential conclusion drawn from the experiments was that the system was capable of drastically reducing the errors caused by prostate mobility in the cranial-caudal direction. This was true for the different depths of insertion and approach angles tested. Although further definitive in vivo studies need to be done, it has been stated in the literature that the primary axis of prostate mobility during brachytherapy is along the needle insertion axis [5], [46].

Although the cranial-caudal direction was the primary axis of mobility, our experiments did, however, confirm that prostate rotation affects the results significantly. During needle

insertion, the target was not only pushed in the z-direction, but also rotated away from the needle insertion axis, making the target unreachable without re-inserting the needle at a different approach angle. The deeper the insertion, the more the prostate rotated. It was also noticed that peripheral needles caused more rotation than central needles, as could be expected. The importance of prostate rotation was made clear during these experiments. An important future step for the success of any prostate needle insertion system would, therefore be to determine the degree to which this occurs in vivo and to provide ways of mitigating this error, such as predicting motion with biomechanical models [47] or reducing prostate motion with stabilizing needles [30].

Regarding the discrepancy between apex and base measurements, this can be explained by the poorer US characteristics at the base: with an end-fire probe, the prostate base is further from the transducers than the apex, resulting in poorer resolution and increased reconstruction and measurement errors. This could be eliminated by the use of a side-fire probe (as mentioned in the probe description section above) which would make the apex and base at approximately equal depths.

It is important to keep in mind that all the results presented include needle rotation at 8 rps. In our own studies using a force sensor mounted to the insertion module of the robot, we found that, at this speed, needle-tissue forces were reduced in the phantom material by 20%. We chose to include rotation in our experiments in order to maximize the effectiveness of our system, all the while keeping the rotation to a very reasonable low speed: evidently high speed rotations would present significant safety issues to the patient.

The effect of rotation on tissue damage is also an important aspect to verify before applying it on real patients. The beginnings of this have been shown in the cadaver study done subsequently. We believe that the tissue damage seen in the cadaver study is a result of the needle type, whose cutting tip was designed for straight insertion, not rotational cutting. Also, we expect this behavior to be different in fresh tissue, which is more supple and irrigated.

Another important aspect to discuss is the use of automatic insertion as opposed to the current standard of manually inserting the needles. The main advantage of automatic needle insertion is its accuracy and repeatability, but in addition, without it, the aforementioned needle rotation would not be possible. It could be argued, though, that clinicians would be hesitant to allow automation of this invasive act for two reasons: 1) patient safety and 2) the loss of tactile feedback during needle insertion. The first reason would evidently require validation and redundancy measures to reduce the risk sufficiently to justify the increase in accuracy obtained. Regardless, it would be necessary to evaluate this clinically. The loss of tactile feedback would not necessarily be a drawback since the needle depth is always known with respect to the prostate, due to the robot-probe calibration.

A final important issue is the effect of needle insertion and progressive seed deposition on image quality and hence on the accuracy of the registration algorithm. The needle traces and seeds could add high intensity regions in the image that could adversely affect the registration between the current "dirty" image and the "clean" reference image. As mentioned in section III.D, the algorithm was originally developed in the context of prostate biopsies, and has been extensively tested on clinical cases [39]. During these clinical trials, certain elements were observed that are to our advantage. Although needle traces after needle removal were very evident in our phantom and cadaver tests, they are, in fact, very rarely observable in the clinical cases, as they fill with liquid (blood), which re-establishes an acoustic connection. Note that during the biopsies we inserted and removed a dozen needles without observing any problem with the algorithm. In addition, the needle volume is very small when compared to the total image volume, making its impact very limited; the registration algorithm is quite robust, in fact, to localized changes in image intensity. As far as needle presence in the image is concerned, our system is based on a single-needle tactic, so only one needle is ever present in the image at a time. Our experiments, as well as the clinical biopsy trials have clearly shown that this does not cause problems for our algorithm. Regardless, since we know the current location of the needle in the image, we can therefore ignore it during registration by applying an image mask [39]. This can also be done for the deposited seeds and will be the subject of a future publication.

VIII. Conclusion and Future Work

In this paper, we presented a new 3D ultrasound robotic brachytherapy system called PROSPER. It uses 3D ultrasound registration of the prostate to track the location of the gland and the dose plan distributed inside it. The robotic needle insertion mechanism and ultrasound system were described in detail, followed by an account of the methods used to calibrate the robot and the 3D TRUS probe. Experiments on synthetic, mobile prostate phantoms were described, showing the system's ability to correct for prostate motion and deformation in the needle insertion direction. A preliminary cadaver feasibility study was also described, in which image registration and needle insertions were verified.

This work has underlined the need for a number of future objectives. To begin with, the robot prototype described in this paper was designed for laboratory use. Before the design could be used in a clinical setting, a few changes would be required. First of all, the weight and size of the prototype, although relatively small as it is, could be reduced. The main bulk of this prototype comes from the off-the-shelf stepper motors used to power the four parallel linear stages. By replacing them with smaller brushless servomotors, this bulk could be significantly decreased. The off-the-shelf linear stages are also not ideal for this application, as the carriages should ideally be stiffer in order to make the robot more robust to user handling. A slightly larger workspace could also be useful, such that higher needle inclination could be achieved throughout the

volume of larger prostates.

The main technical objective that will be undertaken is improving the management of prostate rotations during needle insertion by constraining rotational gland motions through the use of two or three pre-inserted stabilizing needles. An important aspect would also be an in depth clinical study to define how the prostate deforms and moves during needle insertion in vivo. Few detailed and accurate studies exist in the literature that quantify the 6 DOF translations, rotations and deformations that the gland experiences during brachytherapies [5], [6], [46], [48].

Another objective, as mentioned in the previous section, is to determine whether needle rotation is clinically viable in terms of tissue damage. A clinical study of this nature would be very delicate to carry out, so further studies on fresh cadaver or fresh animal tissues would have to be done instead.

Some final improvements will be to complete the sterilization procedure of the robot and to replace the end-fire US probe by a side-fire 3D probe. These improvements will be validated on cadaver tests, and given the encouraging results presented in this paper, we expect to begin preliminary clinical trials soon after.

APPENDIX

The prototype robot used for needle positioning and insertion in our system is based on a parallelogram-type manipulator with two kinematic chains that split at the robot's base and reunite at the robot's needle insertion module. The kinematic diagram of the robot is shown in Figure 16. The DH parameters for the two chains are shown in Table 5.

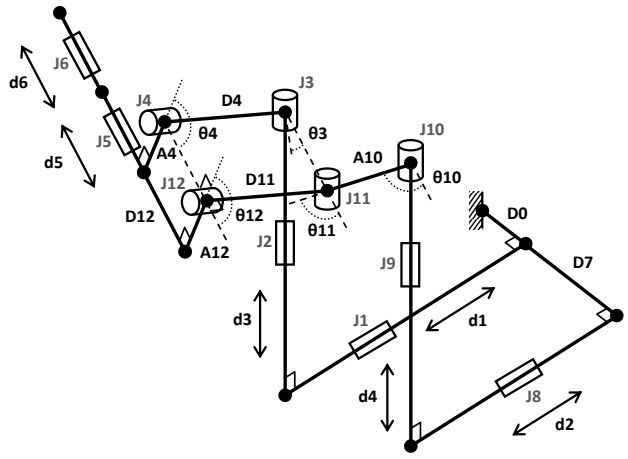

Fig. 16. Kinematic diagram of the prototype robot.

TABLE V
ROBOT DH PARAMETERS

Joint	a_i	d_i	α_i	θ_i
Chain 1:				
0	0	-D0	0	90
1	0	d1 + M1	90	-90
2	0	M3 - d3	-90	0
3	0	0	0	-θ3
4	0	D4	90	θ4
5	-A4	d5 + M5	-90	0
Chain 2:				
7	0	- (D0 + D7)	0	90
8	0	d2 + M2	90	-90
9	0	M4 - d4	-90	0
10	0	0	0	-θ10
11	A10	0	0	θ11
12	0	D11	90	θ12
5	-A12	D12 + d5	-90	0
Insertion Module:				
6	0	d6 + M6	0	-90

All angles in degrees. "M" parameters are motor offsets.

ACKNOWLEDGMENT

The authors would like to gratefully acknowledge the invaluable time, advice and encouragement of our clinical partners at the Grenoble University Hospital (CHU Grenoble), Pr. Michel Bolla, Pr. Jean-Luc Descotes and Jean-Yves Giraud, who requested this project in the beginning to help improve the treatment of their patients. This project was done in partnership with Koelis SAS, La Tronche, France and the prototype was built by Axe Systems, Romorantin, France.

REFERENCES

[1] American Cancer Society. (2012). Cancer Facts and Figures 2012 [Online]. Available: http://www.cancer.org.

[2] Institut National du Cancer (2011, October). La situation du cancer en France en 2011 [Online] http://www.e-cancer.fr

[3] P. Stattin, E. Holmberg, J. E. Johansson, L. Holmberg, J. Adolfsson, and J. Hugosson, "Outcomes in Localized Prostate Cancer: National Prostate Cancer Register of Sweden Follow-up Study," *J. Natl. Cancer. Inst*., vo. 102, no. 13, pp. 950–958, July 2010.

[4] G. L. Lu-Yao, P. C. Albertsen, D. F. Moore, W. Shih, Y. Lin, R. S. DiPaola, M. J. Barry, A. Zietman, M. O'Leary, E. Walker-Corkery, and S. L. Yao, "Outcomes of localized prostate cancer following conservative management," *JAMA*, vol. 302, no. 11, pp. 1202-1209, 2009.

[5] N. N. Stone, J. Roy, S. Hong, Y. C. Lo and R. G. Stock, "Prostate gland motion and deformation caused by needle placement during brachytherapy," *Brachytherapy*, vol. 1, no. 3, pp. 154-160, 2002.

[6] V. Lagerburg, M. A. Moerland, J. J. Lagendijk, and J. J. Battermann, "Measurement of prostate rotation during insertion of needles for brachytherapy," *Radiother. Oncol.*, vol. 77, pp. 318–323, 2005.

[7] S.V. Sejpal, V. Sathiaseelan, I. B. Helenowski, J. M. Kozlowski, M. F. Carter, R. B. Nadler, D. P. Dalton, K. T. McVary, W. W. Lin, J. E. Garnett, and J. A. Kalapurakal, "Intra-operative pubic arch interference during prostate seed brachytherapy in patients with CT-based pubic arch interference of ≤1 cm," *Radiother. Oncol*., vol. 91, no. 2, pp. 249-54, May 2009.

[8] K. Chinzei, N. Hata, F. A. Jolesz, R. Kikinis, "MR Compatible Surgical Assist Robot: System Integration and Preliminary Feasibility Study," in *Int. Conf. Med. Image Comput. Comput. Assist. Interv.*, vol. 3, pp. 921-930, 2000.

[9] G. Fichtinger, T. L. DeWeese, A. Patriciu, A. Tanacs, D. Mazilu, J. H. Anderson, K. Masamune, R. H. Taylor, and D. Stoianovici, "System for robotically assisted prostate biopsy and therapy with intraoperative CT guidance," *Acad. Radiol*., vol. 9, no. 1, pp. 60-74, Jan. 2002.

[10] B. L. Davies, S. J. Harris, and E. Dibble, “Brachytherapy—an example of a urological minimally invasive robotic procedure,” *Int. J. Med. Robot.*, vol. 1, no. 1, pp. 88-96, Jun. 2004.

[11] C. M. Schneider, A. M. Okamura, and G. Fichtinger, "A robotic system for transrectal needle insertion into the prostate with integrated ultrasound," in *Proc. IEEE Int. Conf. Rob. Autom.*, vol. 1, pp. 365-370, 2004.

[12] L. Phee, D. Xiao, J. Yuen, C. F. Chan, H. Ho, C. H. Thng, C. Cheng, and W. S. Ng, "Ultrasound Guided Robotic System for Transperineal Biopsy of the Prostate," in *Proc. IEEE Int. Conf. Rob. Autom.*, pp. 1315- 1320, 2005.

[13] Z. Wei, M. Ding, D. Downey, and A. Fenster, “3D TRUS guided robot assisted prostate brachytherapy,” *Med. Image Comput. Comput. Assist. Interv.*, vol. 8, no. Pt 2, pp. 17-24, 2005.

[14] G. Fichtinger, E. C. Burdette, A. Tanacs, A. Patriciu, D. Mazilu, L. L. Whitcomb, and D. Stoianovici, “Robotically assisted prostate brachytherapy with transrectal ultrasound guidance-Phantom experiments,” *Brachytherapy*, vol. 5, no. 1, pp. 14-26, Jan.-Mar. 2006.

[15] Y. Yu, T. K. Podder, Y. D. Zhang, W. S. Ng, V. Misic, J. Sherman, D. Fuller, D. J. Rubens, J. G. Strang, R. A. Brasacchio, and E. M. Messing, “Robotic system for prostate brachytherapy,” *Comput. Aided Surg.*, vol. 12, no. 6, pp. 366-70, Nov. 2007.

[16] H. Bassan, T. Hayes, R. V. Patel, and M. Moallem, "A Novel Manipulator for 3D Ultrasound Guided Percutaneous Needle Insertion," in *Proc. IEEE Int. Conf. Rob. Autom.*, pp.617-622, April 2007.

[17] T. K. Podder, W. S. Ng; Y. Yu, "Multi-channel robotic system for prostate brachytherapy," in *Proc. 29th Ann. Int. Conf. IEEE Eng. Med. Biol. Soc.*, pp.1233-1236, Aug. 2007.

[18] G. S. Fischer, I. I. Iordachita, C. Csoma, J. Tokuda, S. P. DiMaio, C. M. Tempany, N. Hata, and G. Fichtinger, “MRI-Compatible Pneumatic Robot for Transperineal Prostate Needle Placement,” *IEEE ASME Trans. Mechatron.*, vol. 13, no. 3, pp. 295-305, Jun. 2008.

[19] A. Patriciu, D. Petrisor, M. Muntener, D. Mazilu, M. Schar, and D. Stoianovici, "Automatic Brachytherapy Seed Placement Under MRI Guidance," *IEEE Trans. Biom. Eng.*, vol. 54, no. 8, pp. 1499-1506, Aug. 2007.

[20] G. Fichtinger, J. P. Fiene, C. W. Kennedy, G. Kronreif, I. Iordachita, D. Y. Song, E. C. Burdette, and P. Kazanzides, “Robotic assistance for ultrasound-guided prostate brachytherapy,” *Med. Image Anal*., vol. 12, no. 5, pp. 535-45, Oct 2008.

[21] S. E. Salcudean, T. D. Prananta, W. J. Morris, and I. Spadinger, "A robotic needle guide for prostate brachytherapy," in *Proc. IEEE Int. Conf. Rob. Autom.*, pp. 2975-2981, May 2008.

[22] V. P. Heikkilä, and N. Suorsa, “A technique for simultaneous needle insertion in prostate seed implantation,” *Phys. Med. Biol*., vol. 53, no. 4, pp. N35-N39, 2008.

[23] H. S. Ho, P. Mohan, E. D. Lim, D. L. Li, J. S. Yuen, W. S. Ng, W. K. Lau, and C. W. Cheng, “Robotic ultrasound-guided prostate intervention device: system description and results from phantom studies,” *Int. J. Med. Robot.*, vol. 5, no. 1, pp. 51-58, Mar. 2009.

[24] M. R. van den Bosch, M. R. Moman, M. van Vulpen, J. J. Battermann, E. Duiveman, L. J. van Schelven, H. de Leeuw, J. J. Lagendijk, and M. A. Moerland, “MRI-guided robotic system for transperineal prostate interventions: proof of principle,” *Phys. Med. Biol*., vol. 55, no. 5, pp. N133-140, Mar. 2010.

[25] S. E. Song, N. B. Cho, G. Fischer, N. Hata, C. Tempany, G. Fichtinger, and I. Iordachita, “Development of a Pneumatic Robot for MRI-guided Transperineal Prostate Biopsy and Brachytherapy: New Approaches,” in *Proc. IEEE Int. Conf. Robot. Autom.*, vol. 15, pp. 2580-2585, Jul. 2010.

[26] J. Bax, D. Smith, L. Bartha, J. Montreuil, S. Sherebrin, L. Gardi, C. Edirisinghe, and A. Fenster, “A compact mechatronic system for 3D ultrasound guided prostate interventions,” *Med. Phys*., vol. 38, no. 2, pp. 1055-69, Feb. 2011.

[27] A. Krieger, I. I. Iordachita, P. Guion, A. K. Singh, A. Kaushal, C. Ménard, P. A. Pinto, K. Camphausen, G. Fichtinger, and L. L. Whitcomb, “An MRI-Compatible Robotic System with Hybrid Tracking for MRI-Guided Prostate Intervention,” *IEEE Trans. Biom. Eng.*, vol. 58, no. 11, 2011.

[28] T. K. Podder, D. P. Clark, D. Fuller, J. Sherman, W. S. Ng, L. Liao, D. J. Rubens, J. G. Strang, E. M. Messing, Y. D. Zhang, and Y. Yu, “Effects of Velocity Modulation during Surgical Needle Insertion,” in *Proc. 27th Annu. Conf. IEEE Eng. Med. Biol.*, Shanghai, pp. 5766-5770, 2005.

[29] M. A. Meltsner, N. J. Ferrier, and B. R. Thomadsen, “Observations on rotating needle insertions using a brachytherapy robot,” *Phys. Med. Biol.*, vol. 52, pp. 6027, 2007.

[30] T. Podder, J. Sherman, D. Rubens, E. Messing, J. Strang, W. S. Ng, and Y. Yu, “Methods for prostate stabilization during transperineal LDR brachytherapy,” *Phys. Med. Biol*., vol. 53, no. 6, pp.1563-79, 2008.

[31] M. Ding, Z. Wei, L. Gardi, D. B. Downey, and A. Fenster, “Needle and seed segmentation in intra-operative 3D ultrasound-guided prostate brachytherapy,” in *Proc. Ultrasonics Int. World Congr. Ultrasonics*, vol. 44, Suppl. 1, pp. e331-e336, Dec. 2006.

[32] M. Ding, Z. Wei, D. B. Downey, and A. Fenster, "Automated seed localization for intraoperative prostate brachytherapy based on 3D line segment patterns," in *Proc. SPIE Int. Symp. Med. Im.*, San Diego, vol. 5744, pp. 417-423, 2005.

[33] X. Wen, and S. E. Salcudean SE, “Detection of brachytherapy seeds using 3D ultrasound,” in *Conf. Proc. IEEE Eng. Med. Biol. Soc.*, pp. 855-858, 2008.

[34] J. Bax, D. Cool, L. Gardi, K. Knight, D. Smith, J. Montreuil, S. Sherebrin, C. Romagnoli, and A. Fenster, “Mechanically assisted 3D ultrasound guided prostate biopsy system,” *Med. Phys.*, vol. 35, no. 12, Dec. 2008.

[35] S. Xu, J. Krucker, P. Guion, N. Glossop, Z. Neeman, P. Choyke, A. K. Singh, and B. J. Wood, “Closed-loop control in fused MR-TRUS image-guided prostate biopsy,” *MICCAI*, vol. 4791, pp. 128-135, 2007.

[36] S. Martin, M. Baumann, V. Daanen, and J. Troccaz, “MR prior based automatic segmentation of the prostate in TRUS images for MR/TRUS data fusion,” in *Proc. IEEE ISBI*, Rotterdam, Apr. 2010.

[37] Daanen, V., Gastaldo, J., Giraud, J. Y. et al.: MRI/TRUS data fusion for brachytherapy. Int J Med Robot, **2:** 256, 2006.

[38] N. Hungr, J. Troccaz, N. Zemiti, and N. Tripodi, “Design of an Ultrasound-Guided Robotic Brachytherapy Needle-Insertion System,” in *Proc. 31st Annu. Int. Conf. IEEE Eng. Med. Biol. Soc.*, Minneapolis, pp. 250-253, 2009.

[39] M. Baumann, P. Mozer, V. Daanen, and J. Troccaz, “Prostate biopsy tracking with deformation estimation,” *Med. Im. Anal.*, vol. 16, no. 3, pp. 562-576, Apr. 2011.

[40] M. Baumann, P. Mozer, V. Daanen, and J. Troccaz, “Prostate biopsy assistance system with gland deformation estimation for enhanced precision,” *Med. Image Comput. Comput. Assist. Interv.*, vol. 12, Pt. 1, pp. 67-74, 2009.

[41] M. Baumann, P. Mozer, V. Daanen, and J. Troccaz, “Towards 3D Ultrasound Image based Soft Tissue Tracking: A Transrectal Ultrasound Prostate Image Alignment System,” in *MICCAI*, vol. 4792, pp. 26-33, 2007.

[42] J. A. Long, V. Daanen, A. Moreau-Gaudry, J. Troccaz, J. J. Rambeaud, and J. L. Descotes, “Prostate biopsies guided by three-dimensional real-time (4-D) transrectal ultrasonography on a phantom: comparative study versus two-dimensional transrectal ultrasound-guided biopsies,” *Eur. Urol.*. vol. 52, no. 4, pp. 1097-1104, Oct. 2007.

[43] N. Bilaniuk and G. S. K. Wong, “Erratum: Speed of sound in pure water as a function of temperature,” *J. Acoust. Soc. Am.*, vol. 99, no. 5, p 3257, 1996.

[44] K. S. Arun, T. S. Huang, and S. D. Blostein, “Least-Squares Fitting of Two 3-D Point Sets,” *IEEE Trans. Pattern Anal. Machine Intel.*, vol.PAMI-9, no.5, pp.698-700, Sept. 1987.

[45] N. Hungr, J. A. Long, V. Beix, and J. Troccaz, “A realistic deformable prostate phantom for multi-modal imaging and needle-insertion procedures,” *Med. Phys.*, vol. 39, no. 4, Apr. 2012, to be published.

[46] R. Taschereau, J. Pouliot, J. Roy, and D. Tremblay, “Seed misplacement and stabilizing needles in transperineal permanent prostate implants,” *Radiother. Oncol.*, vol. 55, no. 1, pp. 59-63, Apr. 2000.

[47] E. Dehghan, and S. E. Salcudean, "Needle Insertion Parameter Optimization for Brachytherapy," *IEEE Trans. Rob.*, vol. 25, no. 2, pp. 303-315, Apr. 2009.

[48] T. De Silva, A. Fenster, J. Bax, C. Romagnoli, J. Izawa, J. Samarabandu, and A. D. Ward, “Quantification of prostate deformation due to needle insertion during TRUS-guided biopsy: Comparison of hand-held and mechanically stabilized systems,” *Med. Phys.*, vol. 38, pp. 1718-1731, 2011.

Nikolai Hungr received his Masters of Applied Science (M.A.Sc.) degree in mechanical engineering from the University of British Columbia, Vancouver, in March of 2008. He completed his undergraduate studies at the same university in 2003. During his Masters, he worked on developing new haptic techniques for bone milling in orthopaedic surgery.

After his Masters, he was employed as a research engineer at the Techniques de l'Ingénierie Médicale et de la Complexité (TIMC-IMAG) laboratory in Grenoble, France, until 2010, where he worked on a number of needle insertion robotics projects in the fields of urology and interventional radiology. He is currently in his second year as a PhD student in the same laboratory.

Mr. Hungr has received a number of awards during his studies, including the Natural Sciences and Engineering Research Council of Canada Post Graduate Scholarship.

Michael Baumann received the M.Sc. and M.Eng. degree in computer science in 2004 from the Universität Karlsruhe, TH, Germany, and the INSA de Lyon, France, and the PhD degree in computer science in 2008 from the INP University of Grenoble, France.

From 2006, he has been employed by Koelis SAS, France, and the TIMC laboratory, Grenoble, France. His research interests include medical image processing, image fusion, organ tracking, prostate cancer diagnosis and therapy. He is a specialist for prostate ultrasound imaging, automated prostate tracking, contouring and multimodal prostate image fusion.

Jean-Alexandre Long received his MD degree in 2005 and is currently associate professor in the Urology Department of Grenoble University Hospital.

His research interests are in the urologic oncology field. He is member of the Oncology Group of the French Association of Urology and has been research fellow in the department of minimally invasive surgery at the Cleveland clinic (USA).

He is currently in his 4th year as a PhD student at TIMC lab.

Jocelyne Troccaz was born in 1959. She received a Ph.D. in Computer Science from the Institut National Polytechnique de Grenoble in 1986. She is a CNRS Research Director since 1998.

Until 1990, her activity was in the field of automatic robot programming for industrial and spatial robotics. She moved to Medical Robotics in 1990. Her personal research activity in the TIMC laboratory of Grenoble is about the medical applications of robotics and medical image processing. She is involved in several clinical collaborations. She has over 180 publications including international patents. She has been an invited speaker in several conferences. She is on the organizing committees of a number of international conferences of her former and current research domains. She has been a consultant for robotics companies. She is or has been Associate Editor for the Journal of Computer-Aided Surgery, for the IEEE Transactions on Robotics, for the International Journal of Medical Robotics and Computer-Aided Surgery and she is on the editorial board the Medical Image Analysis Journal. She was elected MICCAI fellow in 2010.

From 1996, she has been Director of the « Computer Assisted Medical Interventions » group (35 people) of the TIMC laboratory. From 2006, she has been vice-director of the TIMC laboratory (180 people).